

Magnetic correlations in $\text{Ho}_x\text{Tb}_{2-x}\text{Ti}_2\text{O}_7$ L. J. Chang,^{1,2,*} W. Schweika,³ Y. -J. Kao,^{4,5} Y. Z. Chou,^{4,6} J. Perbon,³ Th. Brückel,³ H. C. Yang,⁴
Y. Y. Chen,⁷ and J. S. Gardner⁸¹*Department of Physics, National Cheng Kung University, Tainan 70101, Taiwan*²*Quantum Beam Science Directorate, Japan Atomic Energy Agency (JAEA), Tokai, Ibaraki 319-1195, Japan*³*Institut für Festkörperforschung, Forschungszentrum Jülich, DE-52425 Jülich, Germany*⁴*Department of Physics, National Taiwan University, Taipei 106, Taiwan*⁵*Center of Quantum Science and Engineering, National Taiwan University, Taipei 10607, Taiwan*⁶*Department of Physics and Astronomy, Rice University, Houston, Texas 77005, USA*⁷*Institute of Physics, Academia Sinica, Nankang Taipei 115, Taiwan*⁸*Indiana University, 2401 Milo B. Sampson Lane, Bloomington, Indiana 47408, USA*

(Received 1 November 2010; revised manuscript received 17 February 2011; published 18 April 2011)

Polycrystalline samples of $\text{Ho}_x\text{Tb}_{2-x}\text{Ti}_2\text{O}_7$ ($0 < x < 2$) have been prepared and characterized for their structural and magnetic properties. The parent compounds of this solid solution are the spin ice $\text{Ho}_2\text{Ti}_2\text{O}_7$ and the spin liquid $\text{Tb}_2\text{Ti}_2\text{O}_7$. Specific-heat measurements on $\text{HoTbTi}_2\text{O}_7$ ($x = 1.0$) reveal the absence of a long-range order state above 0.5 K. The integrated entropies of all $\text{Ho}_x\text{Tb}_{2-x}\text{Ti}_2\text{O}_7$ specimens up to 30 K scale well with the ratio of spin ice and spin liquid in the composition. The neutron diffraction spectrum of $\text{HoTbTi}_2\text{O}_7$ exhibits a dipolar spin-ice pattern and can be well described by mean-field theory for $\langle 111 \rangle$ Ising spins, nearest-neighbor exchange, and dipolar interactions. Inelastic neutron scattering on $\text{HoTbTi}_2\text{O}_7$ reveals two dispersionless excitations, one of ~ 2.5 meV out of the ground state, and a 4-meV transition out of an excited state. We argue that these data suggest that the very strong single-ion effects of $\text{Ho}_2\text{Ti}_2\text{O}_7$ and $\text{Tb}_2\text{Ti}_2\text{O}_7$ persist in the $\text{Ho}_x\text{Tb}_{2-x}\text{Ti}_2\text{O}_7$ ($0 < x < 2$) solid solution, whereas the Tb-Ho correlations are weak, resulting in small shifts in the energy scales but with no dramatic effect on the bulk properties.

DOI: [10.1103/PhysRevB.83.144413](https://doi.org/10.1103/PhysRevB.83.144413)

PACS number(s): 28.20.Cz, 75.50.-y

I. INTRODUCTION

$\text{A}_2\text{B}_2\text{O}_7$, where A is a rare-earth ion and B is a transition-metal ion, compounds forming a pyrochlore oxide structure have attracted significant attention from both experimental and theoretical physicists in the past two decades owing to their remarkable low-temperature magnetic properties.^{1,2} In pyrochlore oxides, as well as in other geometrically frustrated magnets, a delicate balance between the exchange and dipolar interactions, single-ion anisotropy, and the underlying geometries drives the systems into novel magnetic ground states. These distinguished properties include a spin-glass state with very little, or no, structural disorder,^{3,4} collective paramagnetism or spin-liquid behavior,⁵ and the most interesting and extensively studied behavior of dipolar spin ice.⁶⁻⁹ Among the pyrochlore oxide family, $\text{Ho}_2\text{Ti}_2\text{O}_7$, $\text{Ho}_2\text{Sn}_2\text{O}_7$, $\text{Dy}_2\text{Ti}_2\text{O}_7$, and $\text{Dy}_2\text{Sn}_2\text{O}_7$ have been identified as spin-ice materials and they can be modeled by a spin model with an $\langle 111 \rangle$ Ising-type anisotropy and a net ferromagnetic interaction.⁶⁻¹⁰ $\text{Tb}_2\text{Ti}_2\text{O}_7$ is a fluctuating spin-liquid state at low temperature^{5,11-14} and, to date, there exists no model that can adequately describe all the physical properties observed in $\text{Tb}_2\text{Ti}_2\text{O}_7$.

The magnetic ground states' organizing principles of spin ice require that two spins should point in and two out of each elementary tetrahedron in the lattice occupied by the rare-earth ions. As in water ice, the spin ice has a degeneracy of energetically preferred states that generates a "zero-point" or residual entropy as the temperature approaches absolute zero.¹⁵ This "two-in, two-out" *ice rule* is stabilized by the long-range dipolar interactions associated with the large moments in the system. This explains the recent studies on diluted spin ice (e.g., replacing Ho or Dy with nonmagnetic Y) or stuffed Ho spin-ice materials (adding more rare-earth ions)

where the spin-ice state persists even when the amount of doping is as high as 40%.¹⁵ Similarly, relaxation measurements by neutron spin echo¹⁶ and ac susceptibility¹⁷ showed that spin dynamics in spin-ice compounds is significantly less sensitive to perturbations than one would naively assume. The generally believed scenario for the magnetic correlations in $\text{Ho}_2\text{Ti}_2\text{O}_7$, and other spin ice is that the spins in each tetrahedron slowly relax through spin-flip processes involving the crystal-field excitations until ~ 15 K, below which this is thermally improbable. A thermally independent process continues to drive the system into the locally ordered state of two in, two out, which is completed by ~ 2 K. Below 2 K, the system re-enters a thermally active regime, and this has been associated with the mobility of defects in the ice rules and the dynamics of so-called *magnetic monopoles*.^{18,19}

In $\text{Tb}_2\text{Ti}_2\text{O}_7$, the system remains in a paramagnetic state, albeit sluggish, to temperatures as low as 15 mK, but short-range (~ 5 Å) correlations develop below 100 K, which are characteristics associated with a cooperative paramagnetic or spin-liquid state.^{5,12,14} The Curie-Weiss law fit through the high-temperature susceptibility of $\text{Tb}_2\text{Ti}_2\text{O}_7$ estimates the Tb^{3+} moment of $9.6 \mu_B$, almost the full free moment, and the Curie-Weiss temperature of -19 K.¹² Further studies on the Y diluted $\text{Tb}_2\text{Ti}_2\text{O}_7$ samples successfully estimated the interactions of the crystal field, dipolar, and exchange contributions to the Curie-Weiss temperature as -6 , -2 , and -11 K, respectively.⁵ The Tb^{3+} configuration was proposed as classical Ising spins constrained to point along local $\langle 111 \rangle$ directions with the mutual interactions of longer-range magnetic dipole interactions and near-neighbor antiferromagnetic exchange interactions.^{5,14} Neutron diffraction experiments revealed that the system has developed short-range

antiferromagnetic correlations up to temperatures as high as 100 K,¹² which grow very little in range but increase in volume as the system cools.²⁰ Inelastic neutron scattering and heat-capacity measurements confirmed the first excited and ground states of the system, both doublets, are separated by about 18 K.¹⁴ Heat capacity also reveals a T^2 dependence appropriate of a three-dimensional dynamical system.⁵ The excitation partially softens at the first maximum in the magnetic structure factor when spin-spin correlation appears below 20 K (Refs. 12 and 14), which can be described by a model including single-ion excitations from the ground-state doublet to higher crystal-field levels.²¹

Here we report the studies of the magnetic behaviors of the mixture compounds of spin ice $\text{Ho}_2\text{Ti}_2\text{O}_7$ and spin liquid $\text{Tb}_2\text{Ti}_2\text{O}_7$. After considering the correlations between Ho^{3+} and Tb^{3+} , one would naively expect the spin-ice and spin-liquid states to yield either a long-range order or more realistically a spin-glass state at low temperatures. In fact, a recent magnetothermal study of another spin-ice and spin-liquid mixture²² revealed distinct differences in its properties to that of the parent compounds. However, more studies, including neutron scattering studies, are desirable to address the crystal-field level quantitatively and to determine the true ground-state Hamiltonian. These studies may also address some of the subtle difference between the canonical spin-ice materials, namely, $\text{Ho}_2\text{Ti}_2\text{O}_7$ and $\text{Dy}_2\text{Ti}_2\text{O}_7$.

In our studies, powder x-ray diffraction was employed to ensure a complete reaction and the formation of a pure solid reaction. Magnetization and heat capacity were measured for these mixtures down to ~ 2 K, and their entropies were calculated to investigate the ground state. Inelastic neutron scattering measurements were carried out on the middle composition mixture, namely, $\text{HoTbTi}_2\text{O}_7$, to examine directly the spin dynamics, crystal-field transitions, and other inelastic processes as a function of temperature. The diffraction configuration exhibits liquidlike diffuse scattering pattern at low Q . The results displayed the robustness of both ground states despite the complete mixture of the elements. In hindsight, since both the Ho^{3+} and Tb^{3+} ions are very Ising like, with a strong preference to lie in the $\langle 111 \rangle$ direction, and the solid solutions only relieve the ice rules slightly, while maintaining a significant amount of degeneracy. The mixtures appear to maintain the local properties of the parent compounds, while the exact energy scales are altered slightly due to the ion substitution.

II. EXPERIMENTAL RESULTS AND DISCUSSIONS

A. Sample preparation and characterizations

$\text{Ho}_x\text{Tb}_{2-x}\text{Ti}_2\text{O}_7$ ($x = 1.8, 1.5, 1, 0.5$, and 0.2) polycrystalline samples were synthesized by the conventional solid-state reaction methods. High-purity starting powder materials of Ho_2O_3 , Tb_4O_7 , and TiO_2 were mixed in stoichiometric proportions, heated at 850 °C for 24 h, pressed into pellets, and then sintered at 1150 °C for 48 h. Room-temperature x-ray diffraction, using a copper target and x-rays with a wavelength of 1.5418 Å, was used to determine the nuclear structure and phase purity. No impurity was found in the polycrystalline samples, within sensitivity limits of a few percent, and

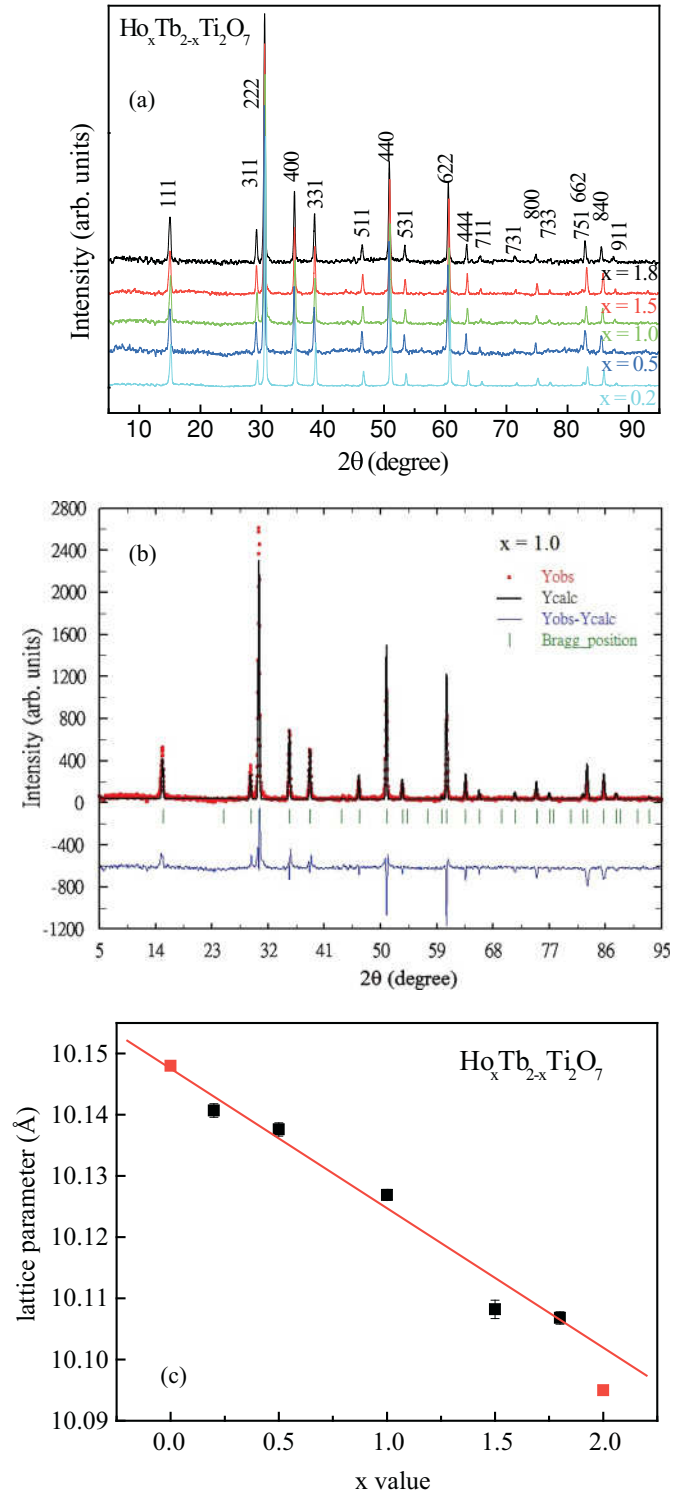


FIG. 1. (Color online) (a) The powder x-ray diffraction pattern and the indexes of main peaks for the $\text{Ho}_x\text{Tb}_{2-x}\text{Ti}_2\text{O}_7$. Each spectrum is offset vertically by a fixed amount for the purpose of clarity. (b) Rietveld refinements of the $x = 1.0$ sample. Data, fits, and Bragg peak positions are shown. (c) The lattice parameters obtained from all the Rietveld refinements for $\text{Ho}_x\text{Tb}_{2-x}\text{Ti}_2\text{O}_7$. The line is a guide for the eye. The data for $x = 0$ and 2 (in red) are taken from Ref. 24.

all samples possessed the face-centered-cubic pyrochlore structure as shown in Fig. 1(a). Rietveld refinements, using

the FULLPROF²³ program, for $x = 1.0$ is shown in Fig. 1(b). The lattice parameters obtained from the Rietvelt refinements of the entire $\text{Ho}_x\text{Tb}_{2-x}\text{Ti}_2\text{O}_7$ series are displayed in Fig. 1(c). The data for $x = 0$ and 2 are taken from Ref. 24. The linear dependence between end members and the fact that no peak splitting was observed indicates that a complete mixing of the cations was achieved in all specimens and no, or very little, phase separation occurred.

B. Magnetization

The magnetic properties were measured by using a commercial superconducting quantum interference device (SQUID) magnetometer between 2–400 K in an applied field of 2 T, and in a temperature range between 2 and 300 K in a smaller applied field of 0.002 T. The inverse dc susceptibility χ^{-1} for each sample is shown in Fig. 2(a). The inset highlights the deviation from the linear Curie-Weiss (CW) behavior at low temperature as the magnetic correlations develop. High-temperature (200–400 K) fits of the susceptibility derive the CW temperatures and the effective paramagnetic moments for $\text{Ho}_x\text{Tb}_{2-x}\text{Ti}_2\text{O}_7$ [these are displayed in Figs. 2(b) and 2(c), respectively]. Unlike $\text{Ho}_2\text{Ti}_2\text{O}_7$, which has a positive CW temperature,²⁵ all $\text{Ho}_x\text{Tb}_{2-x}\text{Ti}_2\text{O}_7$ mixtures show a negative CW temperature elucidating a dominant antiferromagnetic coupling between spins, even in the lightly doped $\text{Ho}_{1.8}\text{Tb}_{0.2}\text{Ti}_2\text{O}_7$. The CW temperatures are all between -14 to -11 K, but, as discussed later, a high-energy crystal-field level can affect these results. The high-temperature paramagnetic moments derived by CW law are shown in Fig. 2(c). The calculated moments vary

smoothly across the solid solution. As mentioned above, results from CW fits are very sensitive to the temperature range used. The CW law also described the data well between 10 ~ 20 K. These data are collected below the temperature appropriate for the lowest crystal-field excitation and, although the calculated effective moments are similar in the two fits, the CW-like temperatures are significantly less antiferromagnetic in nature than those collected at higher temperatures [see Fig. 2(d)]. In fact, the $x = 1.8$ sample has a positive CW temperature such as that seen in the parent compound $\text{Ho}_2\text{Ti}_2\text{O}_7$.²⁶

C. Heat capacity

The low-temperature heat capacity (C_p) was measured using a standard thermal relaxation method between 0.5 to 30 K for $\text{HoTbTi}_2\text{O}_7$. The lattice contribution (C_l) was estimated by scaling the specific-heat curve of $\text{Y}_2\text{Ti}_2\text{O}_7$ (not shown in the figure), and the nuclear Schottky contribution (C_n) was estimated from $\text{Ho}_2\text{GaSbO}_7$.²⁷ The magnetic heat capacity displayed in Fig. 3 shows two anomalies at ~ 17 and ~ 2 K. The broad peak observed at ~ 17 K is reminiscent of a peak seen in $\text{Tb}_2\text{Ti}_2\text{O}_7$ centered approximately at 6 K. This originates from a low-lying crystal field, which is broadened by an exchange correlation field, something seen in many frustrated magnets.⁵ The ~ 11 K (~ 1 meV) difference in the heat-capacity measurements of $\text{HoTbTi}_2\text{O}_7$ and $\text{Tb}_2\text{Ti}_2\text{O}_7$ is also observed in the neutron time-of-flight measurements as shown in Fig. 5(a). It suggests that the local environment around the Tb^{3+} is

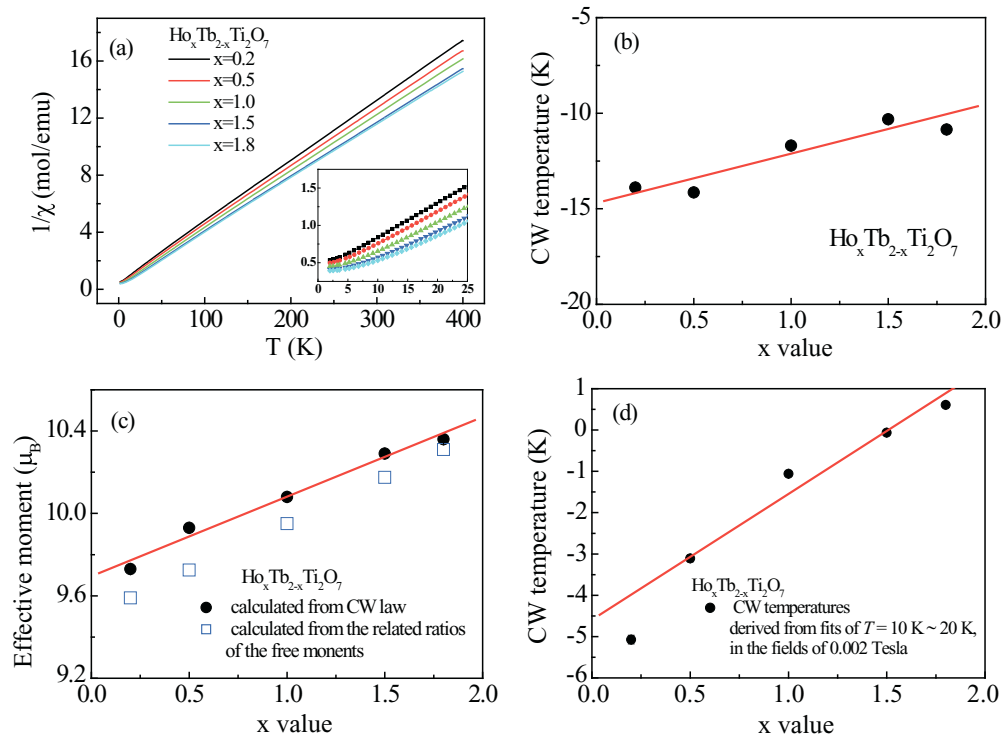


FIG. 2. (Color online) (a) The inverse dc susceptibility χ^{-1} measured at the applied field of 2 T. The inset displays the linear deviation at low temperature, where the magnetic correlations occur; (b) Curie-Weiss (CW) temperatures; and (c) the effective paramagnetic moments derived from CW law at high temperature (200–400 K) ranges for $\text{Ho}_x\text{Tb}_{2-x}\text{Ti}_2\text{O}_7$; (d) CW temperatures estimated by the data between 10 ~ 20 K, and in the applied field of 0.002 T. The error bars derived from CW fits are smaller than the data points. The lines are a guide for the eye.

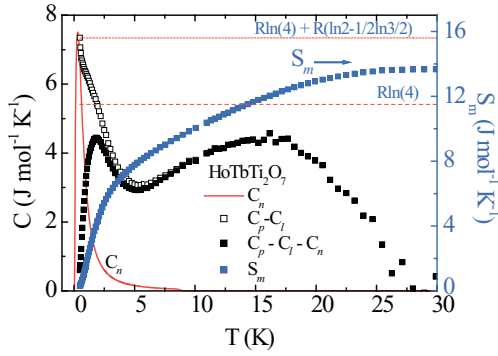


FIG. 3. (Color online) Low-temperature magnetic heat capacity and the accumulated entropy of $\text{HoTbTi}_2\text{O}_7$ up to 30 K. The magnetic heat capacity (C_m) is estimated by subtracting the contributions from lattice (C_l) (not shown in the figure) and nuclear (Schottky) (C_n). The value of accumulated entropy (S_m) is close to $R\ln 4 + R(\ln 2 - 1/2\ln 3/2)$. C_p is the measured, low-temperature, heat capacity.

altered, which is not surprising since Ho^{3+} now occupies half the magnetic sublattices. The heat-capacity peak at ~ 2 K was observed in both $\text{Ho}_2\text{Ti}_2\text{O}_7$ (Ref. 24) and $\text{Tb}_2\text{Ti}_2\text{O}_7$.⁵ The former was explained as the dipolar spin-ice temperature and the latter as the magnetic correlation effect acting on the single-ion ground-state doublet. These two contributions are indistinguishable in our magnetic heat-capacity data. Integrating the magnetic entropy (S_m) of $\text{HoTbTi}_2\text{O}_7$ to 30 K, a value close to $R\ln 4 + R(\ln 2 - 1/2\ln 3/2)$ is obtained. In $\text{Tb}_2\text{Ti}_2\text{O}_7$, the accumulated entropy is just shy of $R\ln 4$ at 30 K for $\text{Tb}_2\text{Ti}_2\text{O}_7$ (Ref. 5) elucidating the presence of four low-lying levels in the spectrum (two doublets), and $R(\ln 2 - 1/2\ln 3/2)$ represents the residual entropy from a two-level system obeying the ice rules, as discussed above and seen in the spin-ice parent compounds.^{9,28} The low-temperature accumulated entropies in other $\text{Ho}_x\text{Tb}_{2-x}\text{Ti}_2\text{O}_7$ compounds are also estimated from their magnetic heat capacities from 2 K up to 30 K, and are listed in Table I. The values roughly scale between those expected for $\text{Tb}_2\text{Ti}_2\text{O}_7$ and $\text{Ho}_2\text{Ti}_2\text{O}_7$. This suggests the strong single-ion anisotropy of the individual rare-earth ions and the preferred local correlations are accommodated in the bulk.

D. Neutron scattering

Neutron scattering experiments have been performed to measure the spin-spin correlations and the inelastic excitations

TABLE I. $\text{Ho}_x\text{Tb}_{2-x}\text{Ti}_2\text{O}_7$ entropies integrated from low-temperature magnetic heat capacities, and the comparisons to the scaled values for $R\ln 4$ and $R(\ln 2 - 1/2\ln 3/2)$. The experimental data are integrated up to 30 K for all the samples.

$\text{Ho}_x\text{Tb}_{2-x}\text{Ti}_2\text{O}_7$		
x	Scaled values for $R\ln 4 + R(\ln 2 - 1/2\ln 3/2)$	Experimental values
0.2	21.56	20.04(3)
0.5	19.38	17.43(2)
1.0	15.60	13.65(3)
1.8	9.64	9.73(1)

while lowering the experimental temperature. These studies, using cold neutron scattering techniques, will help elucidate any low-energy spectral weight, including low-energy crystal-field levels. The experiments were carried out at the former direct time-of-flight spectrometer DNS at the FRJ-II reactor, Jülich, Germany, using neutrons of 4.75 Å wavelength (and 3.6 meV incident energy) with an elastic energy resolution of 0.5 meV (FWHM) and 50 He-3 detectors covering scattering angles up to 135° . A 4.13-g powder sample wrapped in Al foil was mounted in a helium bath cryostat to control the temperatures between 1.5 K and room temperatures. The spectrometer was calibrated using a reference vanadium sample.

1. Elastic neutron scattering and mean-field theory calculation

The elastic neutron scattering from $\text{HoTbTi}_2\text{O}_7$ versus temperature has been obtained by integrating intensities within ± 0.5 meV of 0 energy transfer. Figure 4(a) shows the elastic neutron scattering spectra of different temperatures (lines) and the growths of magnetic correlations, particularly below 50 K with respect to the 150-K data (symbols) from $\text{HoTbTi}_2\text{O}_7$. The scattering at 150 K is essentially paramagnetic apart from large Bragg peaks associated with the chemical structure. In addition, the data appear rather featureless, indicating

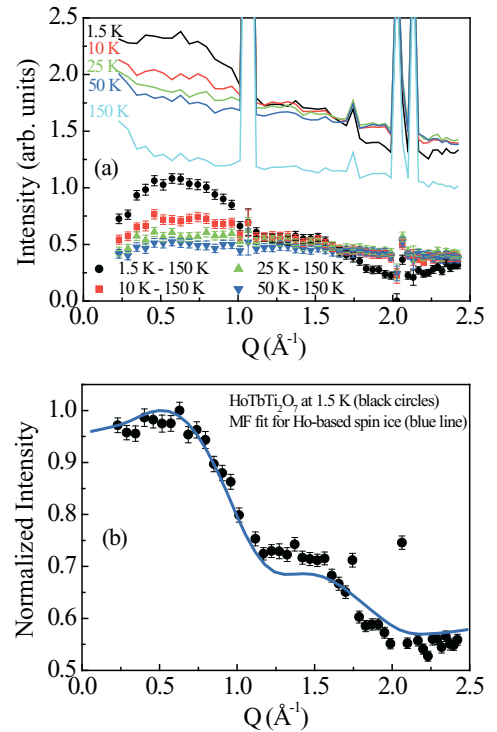


FIG. 4. (Color online) (a) The elastic neutron scattering spectra of different temperatures (lines) and the growths of magnetic correlations, particularly below 50 K, with respect to the 150-K data (symbols) from $\text{HoTbTi}_2\text{O}_7$. At 1.5 K, this broad peak is well developed with a center of mass at $\sim 0.62 \text{ \AA}^{-1}$ and a width $\sim 0.65 \text{ \AA}^{-1}$; (b) the MF dipolar spin-ice fits (line) and the $\text{HoTbTi}_2\text{O}_7$ diffraction spectra (black circles) at 1.5 K. The anomalies at $Q \sim 1.74$ and 2.06 \AA^{-1} are from nuclear peaks. The elastic neutron scattering spectra have been obtained by integrating intensities within ± 0.5 meV of the elastic line.

essentially random spin correlations. Upon cooling to 50 K, more of the spins slow down and the intensity increases. When the temperature is further cooling down, more spin correlations develop and a broad bump appears in the diffraction pattern. The magnetic scattering has a liquidlike structure factor. At base temperature, 1.5 K, it has a broad peak of magnetic scattering with a center of mass at $\sim 0.62 \text{ \AA}^{-1}$ and a (Gaussian) full width of $\sim 0.65 \text{ \AA}^{-1}$ [see Fig. 4(a)]. This low Q diffuse peak suggests that a spin-ice local configuration is dominant in the system. Note, as has been found previously, a mean-field (MF) dipolar spin-ice model predicts the first correlation peak at $\sim 0.59 \text{ \AA}^{-1}$.^{7,29} Therefore, we applied the MF model for dipolar spin ice (described in detail in Ref. 11) to the observed spin correlations. The calculations are based on the dipolar spin-ice model with (111) Ising spins, and contain the nearest-neighbor exchange interactions as well as the long-range dipolar interactions. The Ewald method is employed to obtain the matrix elements of the dipolar interaction matrix.³⁰ The intensity *versus* Q fitted to the $\text{HoTbTi}_2\text{O}_7$ data at 1.5 K uses the equation

$$I(Q) = C[f(Q)]^2 \sum_{\alpha} \frac{|F_{\perp}^{\alpha}(q)|^2}{[1 - \lambda^{\alpha}(q)/T_{\text{MF}}]},$$

where q is a vector in the first Brillouin zone, $F_{\perp}^{\alpha}(q)$ contains information of the spin configurations in the mean-field theory, $\lambda^{\alpha}(q)$ is the eigenvalue of the interaction matrix, C is a proportional constant, and $f(Q)$ is the magnetic form factor.¹¹ When T_{MF} is close to the largest $\lambda^{\alpha}(q)$, the computed intensity shows low-temperature behavior of the spin system. The fitting parameter T_{MF} is 4.92(3) K, and a constant intensity is added as a free parameter in the calculations to account for the background of nonmagnetic origins. The results are displayed in Fig. 4(b). It is clear that this model described the data well, with small remaining discrepancies at $Q \sim 1.2$ and 2.2 \AA^{-1} in the calculations that we cautiously attribute to spin-liquid correlations similar to those seen in $\text{Tb}_2\text{Ti}_2\text{O}_7$.^{11,12} The coexistences of $\text{Ho}_2\text{Ti}_2\text{O}_7$ and $\text{Tb}_2\text{Ti}_2\text{O}_7$ correlations in $\text{HoTbTi}_2\text{O}_7$ indicate weak correlations between Ho^{3+} and Tb^{3+} . The system mainly consists of dipolar stabilized spin-ice correlation and a small number of correlated spin-liquid ions.

2. Inelastic neutron scattering

One advantage of performing time-of-flight measurements with a large detector array is that you get both the elastic and inelastic scattering in the same measurement. The neutron time-of-flight spectra taken at different temperatures are shown in Figs. 5(a)–5(c). Because of the low incident energy (3.6 meV), only low-energy excitations can be observed out of the ground state. A magnetic excitation, out of the ground-state, is observed at ~ 2.5 meV at low temperature [Fig. 5(a)]. This mode is reminiscent of the crystal-field level seen at ~ 1.6 meV in $\text{Tb}_2\text{Ti}_2\text{O}_7$,¹⁴ however, the presence of Ho^{3+} in the compound has shifted the doublet to a higher energy, consistent with the specific-heat results discussed earlier. In addition, unlike the correlated spin liquid $\text{Tb}_2\text{Ti}_2\text{O}_7$, this mode does not soften at any wave vector. This excited mode is washed out at elevated temperature owing to the thermal population; however, it is seen on the negative energy side, corresponding to a neutron energy gain and satisfying detailed balance [Fig. 5(b)]. At 150 K [Fig. 5(c)], another energy level arises at ~ 1.5 meV. The temperature and $|Q|$ dependence of this mode confirms that it is a transition between two excited crystal-field levels. In fact, a similar mode has been observed in $\text{Ho}_2\text{Ti}_2\text{O}_7$ at high temperatures.³¹ In Fig. 5(d), we show the subtractions of 150–20 K. With this background correction, a second $|Q|$ independent mode can be seen on the neutron energy gain side of the spectrum at $\hbar\omega = -4$ meV. No other excitations are observed below 12 meV. The lack of dispersion in the lowest excitation of $\text{HoTbTi}_2\text{O}_7$ suggested the spin-spin correlations are not as developed as those in $\text{Tb}_2\text{Ti}_2\text{O}_7$. This is probably a result of the underlying competition to comply with the local ice rule configuration.

Ke *et al.* recently reported on a similar study on the dysprosium analog of the spin ice.²² In this $\text{Dy}_{2-x}\text{Tb}_x\text{Ti}_2\text{O}_7$ study, the broad peak observed in heat capacity at ~ 6 K in $\text{Tb}_2\text{Ti}_2\text{O}_7$ shifts to a higher temperature for $\text{DyTbTi}_2\text{O}_7$ (~ 10 K) and even higher in our study of $\text{HoTbTi}_2\text{O}_7$ (~ 17 K). This peak is interpreted as a Schottky anomaly resulting from the excited doublet that is “broadened” by exchange correlation fields. As Ke *et al.* concluded, these results suggest that the mixing of the rare-earth site results in an altered crystal-field scheme. This has been confirmed in our neutron inelastic scattering measurements where the

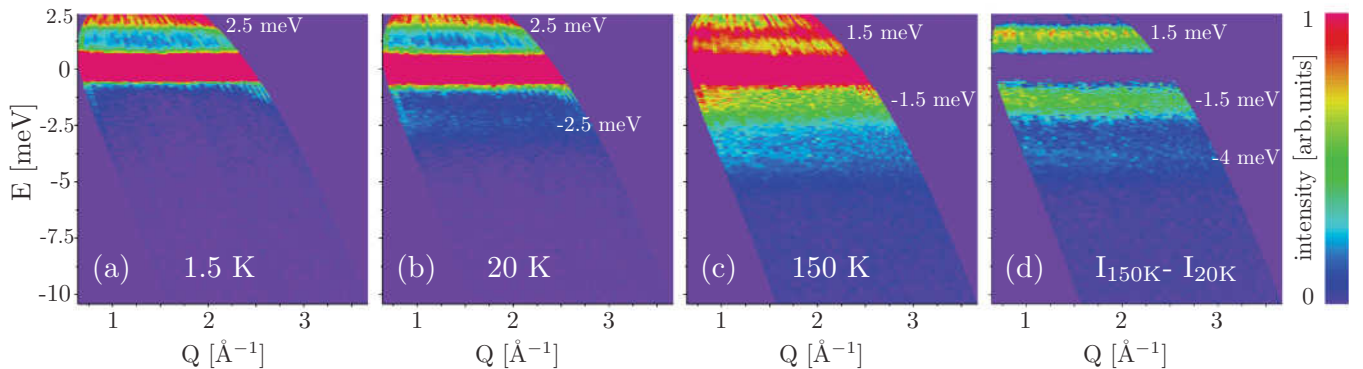


FIG. 5. (Color online) Neutron time-of-flight spectra for $\text{HoTbTi}_2\text{O}_7$ at (a) 1.5 K; (b) 20 K; (c) 150 K; (d) difference of intensities at 150 and 20 K. A 2.5-meV transition out of the ground state is found at low temperatures. 1.5- and 4-meV transitions between excited states are observed when the temperature is elevated and the excited states are thermally populated.

lowest excitation seen at 1.6 meV in $\text{Tb}_2\text{Ti}_2\text{O}_7$ almost doubles to 2.5 meV in $\text{HoTbTi}_2\text{O}_7$. However, we believe the spin interactions are not perturbed significantly. The width of this peak in $\text{Tb}_2\text{Ti}_2\text{O}_7$ and $\text{DyTbTi}_2\text{O}_7$ are similar, and indicate that the exchange correlations between rare-earth ions are similar⁵ and may have actually weakened since there is no dispersion in the inelastic spectra. One must remember that when Tb ions are exchanged for Ho or Dy, the local structure changes because of the change in ionic radii ($\text{Tb}^{3+} > \text{Dy}^{3+} > \text{Ho}^{3+}$), which, in turn, will alter the splitting of the $2J + 1$ degenerate ground state of the rare-earth ions.

From a spin-ice perspective, the long-range dipole-dipole interaction of spin-ice correlations is not disturbed significantly by the diluted Tb ions since the lattice parameter does not change significantly. However, the Curie-Weiss constant becomes more negative and, thus, the exchange constant will change. This will drive the system towards the $Q = 0$ antiferromagnetic state calculated by den Hertog and Gingras.³²

III. CONCLUSIONS

In conclusion, polycrystalline samples of $\text{Ho}_x\text{Tb}_{2-x}\text{Ti}_2\text{O}_7$ have been synthesized and characterized by the powder x-ray diffraction, specific-heat, magnetization, and neutron scattering measurements. The CW temperatures estimated from the magnetization measurements are of reasonable values compared to the values of parent compounds $\text{Ho}_2\text{Ti}_2\text{O}_7$ and $\text{Tb}_2\text{Ti}_2\text{O}_7$, and no magnetic long-range order was observed above 2 K. Specific-heat measurements demonstrate that a possible ground state of the system is a mixture of $\text{Ho}_2\text{Ti}_2\text{O}_7$ and $\text{Tb}_2\text{Ti}_2\text{O}_7$. The low-temperature accumulated entropies scale to the appropriate ratio values of $R\ln 4$ for $\text{Tb}_2\text{Ti}_2\text{O}_7$ and $R(\ln 2 - 1/2\ln 3/2)$ for $\text{Ho}_2\text{Ti}_2\text{O}_7$. No long-range ordering was observed from the specific-heat measurements down to the temperature of 0.5 K in the 50% mixture $\text{HoTbTi}_2\text{O}_7$. Neutron scattering $S(Q)$ has shown that the correlation in $\text{HoTbTi}_2\text{O}_7$ is short ranged and has a tendency for the local spin-ice structure at low temperature ~ 20 K. Inelastic neutron scattering experiments on $\text{HoTbTi}_2\text{O}_7$ show the first excited

doublet at ~ 2.5 meV and the transitions between high-energy excited states at ~ 1.5 and ~ 4 meV. The former can be traced directly to the single-ion properties of Tb^{3+} and the latter is reminiscent to excitation in $\text{Ho}_2\text{Ti}_2\text{O}_7$. The results confirmed the conclusions from the specific-heat measurements, that is, the data can be interpreted as an ensemble of $\text{Ho}_2\text{Ti}_2\text{O}_7$ and $\text{Tb}_2\text{Ti}_2\text{O}_7$ energy levels. The solid solutions of $\text{Ho}_x\text{Tb}_{2-x}\text{Ti}_2\text{O}_7$ possess the local character of both $\text{Ho}_2\text{Ti}_2\text{O}_7$ and $\text{Tb}_2\text{Ti}_2\text{O}_7$ in the specific-heat and neutron scattering measurements. The coexistence of Ho^{3+} and Tb^{3+} alters the precise energy scales of each other but not the bulk properties. In hindsight, these results are not too surprising if one considers the local, single-ion properties of both Ho^{3+} and Tb^{3+} on the pyrochlore lattice. The local environment results in the rare-earth ions having a strong preference to lie along the local $\langle 111 \rangle$ axes. In $\text{Tb}_2\text{Ti}_2\text{O}_7$, it is still not clear why this leads to a spin-liquid ground state, but the net ferromagnetic coupling in $\text{Ho}_2\text{Ti}_2\text{O}_7$ leads to the spin-ice state. Both these states have a considerable amount of degeneracy. Here, we are doping $\text{Tb}_2\text{Ti}_2\text{O}_7$, say, with a spin that wants to lie on the same axes but might want a different configuration of nearest neighbors. The liquid ground state of $\text{Tb}_2\text{Ti}_2\text{O}_7$ can clearly accommodate this perturbation. In $\text{Ho}_2\text{Ti}_2\text{O}_7$, the long-range dipole-dipole correlation makes the system insensitive to the defects in the compound, and thus persists in the spin-ice state.^{16,33} Terbium doping, at least lightly, can be considered a defect that facilitates the emergence of quasiparticles known as magnetic monopole.^{18,19} These elemental excitations are defects in the two-in, two-out spin configuration on a given tetrahedron. Tb doping would probably relax this constraint, but this idea should be examined further with low-temperature heat-capacity measurements on well-characterized samples.

ACKNOWLEDGMENT

This work was supported in Taiwan by Grants No. NSC 96-2739-M-213-001, No. NSC 99-2112-M-007-020 (LJC), No. NSC 97-2628-M-002-011-MY3, and No. NTU 98R0066-65,-68 (Y.Z.C. and Y.J.K.).

*Corresponding author: ljchang@mail.ncku.edu.tw

¹J. S. Gardner, M. J. P. Gingras, and J. E. Greedan, *Rev. Mod. Phys.* **82**, 53 (2010).

²See, *Frustrated Spin System*, edited by H. T. Diep (World Scientific, Singapore, 2004); J. E. Greedan, *J. Alloys Compd.* **408–412**, 444 (2006).

³J. S. Gardner, B. D. Gaulin, S.-H. Lee, C. Broholm, N. P. Raju, and J. E. Greedan, *Phys. Rev. Lett.* **83**, 211 (1999).

⁴D. K. Singh, J. S. Helton, S. Chu, T. H. Han, C. J. Bonnoit, S. Chang, H. J. Kang, J. W. Lynn, and Y. S. Lee, *Phys. Rev. B* **78**, 220405 (2008).

⁵M. J. P. Gingras, B. C. den Hertog, M. Faucher, J. S. Gardner, S. R. Dunsiger, L. J. Chang, B. D. Gaulin, N. P. Raju, and J. E. Greedan, *Phys. Rev. B* **62**, 6496 (2000).

⁶M. J. Harris, S. T. Bramwell, D. F. McMorrow, T. Zeiske, and K. W. Godfrey, *Phys. Rev. Lett.* **79**, 2554 (1997).

⁷H. Kadowaki, Y. Ishii, K. Matsuhira, and Y. Hinatsu, *Phys. Rev. B* **65**, 144421 (2002).

⁸K. Matsuhira, Y. Hinatsu, K. Tenya, and T. Sakakibara, *J. Phys. Condens. Matter* **12**, L649 (2000).

⁹A. P. Ramirez, A. Hayashi, R. J. Cava, R. Siddharthan, and B. S. Shastry, *Nature (London)* **399**, 333 (1999).

¹⁰X. Ke, B. G. Ueland, D. V. West, M. L. Dahlberg, R. J. Cava, and P. Schiffer, *Phys. Rev. B* **76**, 214413 (2007).

¹¹M. Enjalran and M. J. P. Gingras, *Phys. Rev. B* **70**, 174426 (2004).

¹²J. S. Gardner, S. R. Dunsiger, B. D. Gaulin, M. J. P. Gingras, J. E. Greedan, R. F. Kiefl, M. D. Lumsden, W. A. MacFarlane, N. P. Raju, J. E. Sonier, I. Swainson, and Z. Tun, *Phys. Rev. Lett.* **82**, 1012 (1999).

¹³H. R. Molavian, M. J. P. Gingras, and B. Canals, *Phys. Rev. Lett.* **98**, 157204 (2007).

- ¹⁴J. S. Gardner, B. D. Gaulin, A. J. Berlinsky, P. Waldron, S. R. Dunsiger, N. P. Raju, and J. E. Greedan, *Phys. Rev. B* **64**, 224416 (2001).
- ¹⁵G. C. Lau, R. S. Freitas, B. G. Ueland, B. D. Muegge, E. L. Duncan, P. Schiffer, and R. J. Cava, *Nat. Phys.* **2**, 249 (2006).
- ¹⁶G. Ehler, J. S. Gardner, C. H. Booth, M. Daniel, K. C. Kam, A. K. Cheetham, D. Antonio, H. E. Brooks, A. L. Cornelius, A. T. Bramwell, J. Lago, W. Haeussler, and N. Rosov, *Phys. Rev. B* **73**, 174429 (2006).
- ¹⁷J. Snyder, B. G. Ueland, Ari Mizel, J. S. Slusky, H. Karunadasa, R. J. Cava, and P. Schiffer, *Phys. Rev. B* **70**, 184431 (2004).
- ¹⁸C. Castelnovo, R. Moessner, and S. L. Sondhi, *Nature (London)* **451**, 42 (2008).
- ¹⁹L. Jaubert and P. C. Holdsworth, *Nat. Phys.* **5**, 258 (2009).
- ²⁰J. S. Gardner, A. Keren, G. Ehlers, C. Stock, Eva Segal, J. M. Roper, B. Fåk, M. B. Stone, P. R. Hammar, D. H. Reich, and B. D. Gaulin, *Phys. Rev. B* **68**, 180401 (2003).
- ²¹Y.-J. Kao, M. Enjalran, A. D. Maestro, H. R. Molavian, and M. J. P. Gingras, *Phys. Rev. B* **68**, 172407 (2003).
- ²²X. Ke, D. V. West, R. J. Cava, and P. Schiffer, *Phys. Rev. B* **80**, 144426 (2009).
- ²³FULLPROF suite web [<http://www.ill.eu/sites/fullprof/>].
- ²⁴L. H. Brixner, *Inorg. Chem. (Washington, DC)* **3**, 1065 (1964).
- ²⁵S. T. Bramwell, M. N. Field, M. J. Harris, and I. P. Parkin, *J. Phys. Condens. Matter* **12**, 483 (2000).
- ²⁶S. T. Bramwell, M. J. Harris, B. C. den Hertog, M. J. P. Gingras, J. S. Gardner, D. F. McMorrow, A. R. Wildes, A. L. Cornelius, J. D. M. Champion, R. G. Melko, and T. Fennell, *Phys. Rev. Lett.* **87**, 047205 (2001).
- ²⁷H. W. J. Bloete, R. F. Wierlinga, and W. J. Huiskamp, *Physica (Amsterdam)* **43**, 549 (1969).
- ²⁸S. T. Bramwell and M. J. P. Gingras, *Science* **294**, 1495 (2001).
- ²⁹H. D. Zhou, C. R. Wiebe, J. A. Janik, L. Balicas, Y. J. Yo, Y. Qiu, J. R. D. Copley, and J. S. Gardner, *Phys. Rev. Lett.* **101**, 227204 (2008).
- ³⁰P. P. Ewald, *Ann. Phys.* **369**, 253 (1921); S. W. de Leeuw, J. W. Perram, and E. R. Smith, *Rev. Phys. Chem. Jpn.* **37**, 245 (1986).
- ³¹S. Rosenkranz, A. P. Ramirez, A. Hayashi, R. J. Cava, R. Siddharthan, and B. S. Shastry, *J. Appl. Phys.* **87**, 5914 (2000).
- ³²B. C. den Hertog and M. J. P. Gingras, *Phys. Rev. Lett.* **84**, 3430 (2000).
- ³³L. J. Chang, Y. Su, Y.-J. Kao, Y. Z. Chou, R. Mittal, H. Schneider, Th. Brückel, G. Balakrishnan, and M. R. Lees, *Phys. Rev. B* **82**, 172403 (2010).